ACS OMEGA

Open Access

http://pubs.acs.org/journal/acsodf

Article

Mechanistic Study on the Influence of Wax on Hydrate Formation Process

Jinghua Chen, Huiyong Liang,* Haihong Chen, Shi Shen, Haiyuan Yao, Rui Qin, Yang Ge, Ting Huang, and Xin Lv*

Cite This: *ACS Omega* 2024, 9, 31173−31184

Read Online

ACCESS | Metrics & More | Article Recommendations

ABSTRACT: To manage the interactions between wax and hydrate formation, a comprehensive understanding of the system's thermodynamics and flow characteristics is essential. Wax and hydrates coexist under low-temperature and high-pressure conditions, mutually influencing each other both thermodynamically and kinetically. This study focused on two main aspects: how wax affects the rate of hydrate formation in the oil−water system and how hydrate formation influences the thermodynamics of wax crystal precipitation. The presence of wax decreased the rate of hydrate formation, especially at higher wax contents. In systems with high wax content, over 70% of wax precipitated before hydrate formation, leading to less precipitation within the hydrate formation temperature range. With low water content, there were more nucleation sites for wax crystals in the oil phase, resulting in a greater difference in precipitation rates among different wax contents. For water content greater than 10%, the differences in precipitation rates were less significant, indicating a diminished effect of water content on wax crystal precipitation rates. Hydrates' hydrophilic nature had a limited impact on wax crystal nucleation and growth. Generally, wax crystals precipitate before hydrate formation, necessitating control measures for wax deposition during production processes.

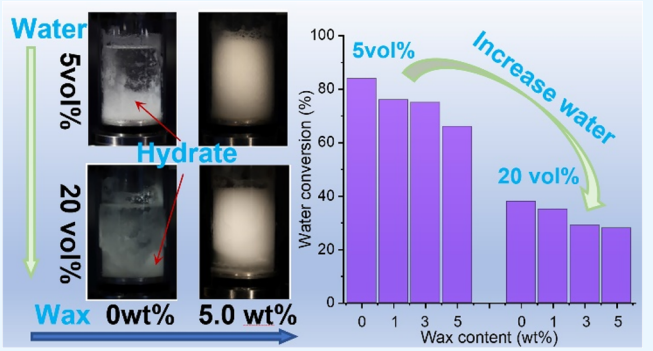

1. INTRODUCTION

Waxes are organic compounds in the oil industry that precipitate from crude oil under certain conditions, particularly during transportation and storage, which has been a significant challenge in the oil industry.[1,2] Crude oil contains various hydrocarbons, some of which have higher melting points than others.[3] As the temperature decreases during transportation or storage, the hydrocarbons with higher melting points solidify and form waxy deposits. These deposits clog the pipelines, equipment, and storage tanks, and thereby decrease the flow rates, the maintenance of which can be potentially costly.[4] At the same time, the precipitation of these sediments promotes the emergence of a new solid substance known as gas hydrate.[5] Hydrates are solid crystalline compounds formed by the combination of water with certain gases, most notably methane.[6,7] In oil and gas industry, methane hydrates are very common and problematic.[8] Methane hydrates typically form at low temperatures and high pressures, making them susceptible in deep-sea oil and gas pipelines.[9,10] Hydrates are formed when the natural gas contains significant amounts of water vapor and the temperature and pressure drop below certain thresholds.[11] These hydrates clog the pipelines and restrict the flow. The formation of hydrates poses significant safety and operational risks in the oil and gas industry.[12]

During the development of offshore oil fields, low-temperature and high-pressure environments in submarine oil pipelines favor the formation of hydrates in oil pipelines.[13] Pressure fluctuations, temperature drops, interceptions, or sudden changes in flow direction can accelerate the formation of hydrates, which damages the oil pipelines and wellhead gathering pipelines. Blockages seriously affect normal production and safe operation of the gas gathering station.[14] In addition to these, crude oil and its components also have an impact on hydrate formation. For crude oil with high wax content, codeposition of hydrates and wax may occur, which would make it more difficult to prevent the deposition of solid phase and blockage.[15,16] In subsea pipelines and flowlines, wax deposition and hydrate formation can occur together, causing

Received: May 24, 2024
Revised: June 17, 2024
Accepted: June 28, 2024
Published: July 5, 2024

issues with flow.[17] Understanding of the interactions between wax deposition and hydrate formation is essential for the mitigation of these problems.

The interactions between wax deposition and hydrate formation would occur in the oil and gas industry, particularly in subsea production systems and pipelines, where conditions conducive to both wax deposition and hydrate formation are present. Although these two phenomena are different, they can influence each other in several ways:

Temperature Effects. The processes of both wax and hydrate formation are highly temperature-dependent. Lower temperatures are favorable for the formation of both wax and hydrates. The temperatures in subsea environments are typically low and there is an increased risk of simultaneous formation of both wax and hydrates.[18]

Flow Assurance Challenges. Deposition of wax and hydrates in pipelines, leading to flow assurance challenges. The presence of one type of deposit can exacerbate the problem of formation of the other.[19] For example, hydrate crystals can provide nucleation sites for wax deposition and accelerate the buildup of wax.[20] On the other hand, wax deposits can create rough surfaces that trap water and promote hydrate formation.[21]

Chemical Treatment Interactions. Chemical inhibitors used to mitigate the deposition of either wax or hydrate crystals might also affect the formation of the other.[22,23] For instance, certain thermodynamic hydrate inhibitors (THIs) impact wax deposition by altering the oil−water interfacial tension.[24] Conversely, wax inhibitors also may alter the water phase behavior, affecting the kinetics of hydrate formation.[25]

Operational Strategies. Operational strategies aimed at preventing one type of deposition may inadvertently worsen the formation of the other. For example, increase of temperature to prevent hydrate formation can potentially bring about melting of wax deposits, which then can accumulate elsewhere in the system.[26]

Managing the interactions between wax and hydrate formation requires a comprehensive understanding of the thermodynamics and flow characteristics of the system. Integrated flow assurance strategies, which combine chemical treatments,[23,27] insulation,[28,29] and operational measures,[13] are often employed to simultaneously mitigate the risks associated with the deposition of both wax and hydrates. Computational modeling[30] and experimental studies play crucial roles in the optimization of these strategies to ensure safe and efficient operation of oil and gas production systems. The focus of this study was on two aspects: the effect of wax on the rate of hydrate formation in the oil−water system and the effect of hydrate formation on the thermodynamics of precipitation of wax crystals.

2. EXPERIMENTAL SECTION

2.1. Materials. Methane (>99.99%) was used in this work to produce form hydrates. The wax used in this work was extracted from crude oil obtained from the X Oilfield in China. The composition of mineral oil used in this work is presented in Table 1.

2.2. Experimental Device. The device used for conducting the experiments is shown in Figure 1. The device consisted mainly of a 316 L stainless steel blind kettle and a reaction kettle. The design pressure was 20 MPa, and the total volume of the kettle and the connected pipeline was 126.4 cm^3. The blind kettle was used to precool the methane gas and prevent the temperature of the reaction system from increasing rapidly when methane is charged into the reaction kettle. The reactor included an upper stainless steel tube and a lower sapphire tube. The upper stainless steel pipe was 7.6 cm long and had a maximum working pressure of 10 MPa. The lower transparent sapphire pipe was manufactured by DB Robinson, Canada, and had a maximum working pressure of 20 MPa. The stainless steel pipe section and the sapphire kettle tube were sealed by an O-ring and a PTFE ring. The temperature fluctuations of the air bath were less than 0.5 °C. The pressure sensor operated in the range of 0−20 MPa with an accuracy of 0.1%. The measurement of oil−water system concentration under different wax concentration by using the HM-ND kinematic viscometer, Shandong Hengclass Electronic Technology Co.

Table 1. Composition of Mineral Oil Used in This Work

Carbon number	Weight percent (%)	Carbon number	Weight percent (%)
C_{17}	1.8	C_{24}	8.3
C_{18}	3.4	C_{25}	13.6
C_{19}	3.9	C_{26}	16.1
C_{20}	5.8	C_{27}	11.2
C_{21}	6.2	C_{28}	5.8
C_{22}	6.2	C_{29}	5.7
C_{23}	6.7	C30	3.6

2.3. Experimental Methods. *2.3.1. Experimental Method for Determination of Methane Hydrate Phase Equilibrium in Waxy Oil−Water Systems.* The temperatures and pressures at which the formation of hydrates occurred in the presence of wax components, resins, and asphaltenes in crude oil were determined by direct visual observation and pressure search method in the high-pressure transparent sapphire autoclave, as shown in Figure 2. The ten compositions for the experiments included: white oil + water systems with varying wax content, resin content, and asphaltene content, as well as water-containing crude oil systems. The water content was fixed at 10 vol %, while the wax contents were 2.0, 4.0, and 8.0 wt %, asphaltene contents were 0.35, 0.7, and 1.4 wt %, and the resin contents were 0.15, 0.3, and 0.6 wt %. The mass fractions mentioned above were all based on the mass of water. The temperature−pressure conditions for hydrate formation were measured twice and the average value was noted.

The steps for determining the hydrate phase equilibrium conditions in wax-simulated crude oil were as follows:

(1) In 18 mL of white oil, 2.0 wt % (or 8.0 wt %) wax (based on oil) was added and the liquid was stirred at 1000 rpm for 1 h, until the wax dissolved completely, followed by the addition of 2 g of water, forming the wax-simulated crude oil.
(2) The simulated crude oil was poured into a high-pressure transparent sapphire autoclave, then the sapphire autoclave was installed in an air bath and stirred at 200 rpm.
(3) The air bath was turned on and the temperature set to 0.5 °C, the buffer tank was filled with sufficient amount of methane, and the methane was precooled.
(4) After about 3 h, the temperature of the oil and water in the sapphire autoclave reached the set value and then the sapphire autoclave was filled with methane to 6.0 MPa pressure from the buffer tank. After about 3 h, hydrates were formed in large quantities.

https://doi.org/10.1021/acsomega.4c04920
ACS Omega 2024, 9, 31173−31184

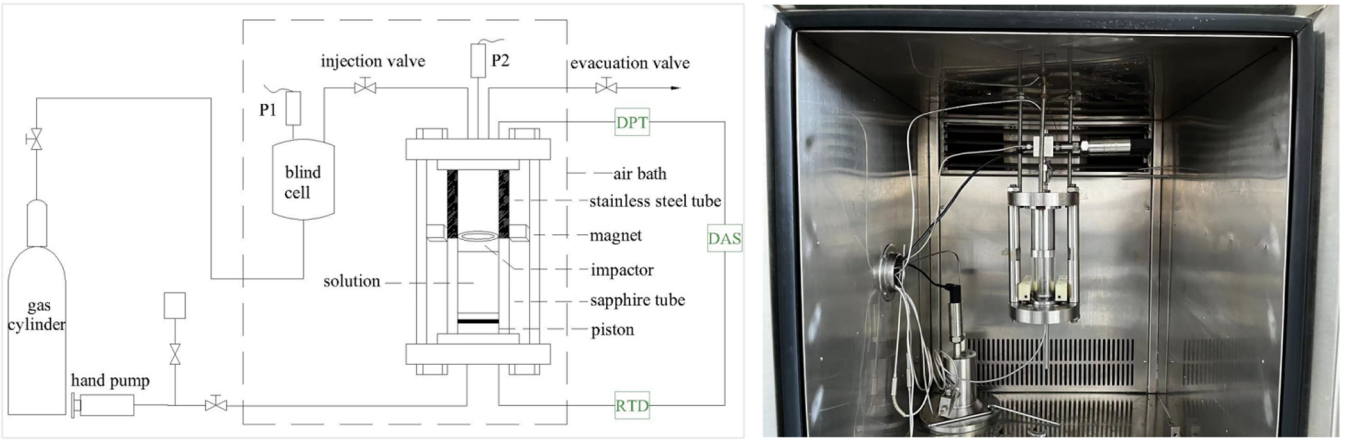

Figure 1. Schematic diagram and actual picture of the experimental device.

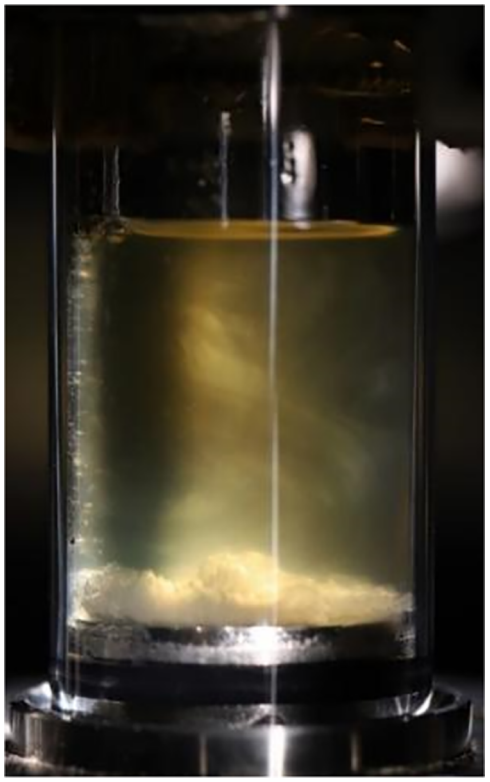

Figure 2. Composition of water generated while determining the conditions of phase equilibrium in a sapphire kettle.

(5) Using the phase equilibrium of methane hydrates in pure water as reference, the pressure in the sapphire autoclave was reduced to the equilibrium pressure of the methane hydrate phase in the pure water system at the same temperature plus 0.5 MPa. Then, it was observed whether the hydrates decomposed and after 10 min, the changes in the trend of pressure curve were observed.

(6) Based on the trend of pressure changes from 10 to 40 min and visual observation of hydrate changes, it was determined whether the hydrates were decomposing. For example, if the pressure curve rose and tiny bubbles appeared on the hydrates, the hydrates were considered to be decomposing. Conversely, if the pressure curve dropped, it was considered that the hydrates were still forming.

(7) Based on the changes in the state of hydrate, it was decided whether to introduce air into the reaction vessel or reduce the pressure of the reaction vessel. If hydrates were still getting formed, the pressure of the reaction vessel was reduced by 0.2 MPa. Alternatively, air was introduced into the reaction vessel to increase the pressure by 0.2 MPa.

(8) Considering the time of air introduction or exhaust as zero point of time, the state of hydrates within the 10 to 40 min interval was reevaluated.

(9) Steps (6) to (8) were repeated until the difference between the end point of the descending curve and the rising curve was less than 30 kPa, which indicated that the hydrates attained equilibrium.

(10) The temperature of air bath was increased by 0.5 °C and steps (4) to (9) were repeated until the methane hydrate phase equilibrium pressure was measured for 15 temperature points.

2.3.2. Experimental Method for Hydrate Formation in Waxy Oil–Water Systems. Steps for the preparation of oil–water mixtures with different wax contents and water contents at 60 °C were as follows:

(1) Oil–water mixtures (20 mL) were prepared with varying wax contents and water contents at 60 °C and then the oil–water mixture was cooled to room temperature.

(2) The prepared oil–water mixture was transferred to the reaction vessel and the vessel sealed. The air bath was started, and the experimental temperature set to 2 °C, stirred at 200 rpm.

(3) The blind vessel and connected pipelines were evacuated to remove air and then sufficient amount of methane gas (>9.0 MPa) was introduced into the blind vessel.

(4) Once the pressure in the blind vessel was stabilized for 0.5 h, which indicated temperature stability of the air bath, the gas pressure inside the blind vessel $P_{b,0}$ was noted. The reaction vessel was evacuated, stirring stopped, the inlet valve opened, 6 MPa of methane gas was introduced into the reaction vessel, and then stirring was resumed.

(5) When the pressure inside the sapphire autoclave was stabilized, which indicated the completion of hydrate formation, the pressures $P_{b,1}$ and $P_{k,1}$ inside the blind vessel and sapphire autoclave, respectively, were noted.

(6) The exhaust valve was opened, stirring maintained, and all the gases from the reaction vessel were evacuated.

https://doi.org/10.1021/acsomega.4c04920
ACS Omega 2024, 9, 31173−31184

The sapphire autoclave was removed, the waste liquid collected, the sapphire autoclave cleaned, and the experiment was complete.

2.3.3. Method for the Determination of Solubility of Methane in White Oil.

(1) White oil (10 mL) was taken in the reaction vessel, and the vessel was sealed and evacuated under vacuum.
(2) The air bath was started and the experimental temperature was set to 2 °C, followed by stirring at 200 rpm.
(3) The blind vessel was filled with methane to 0.2 MPa and then evacuated. This process was repeated twice to remove any air from the blind vessel. Next, the blind vessel was filled with methane to a certain pressure.
(4) Once the pressure in the blind vessel was stabilized, the pressure value $P_{a,0}$ was recorded. The reaction vessel was evacuated and the inlet valve opened to introduce methane into the reaction vessel at a certain pressure.
(5) After the pressure in the sapphire autoclave remained stable for 0.5 h, the pressure values $P_{a,1}$ in the blind vessel and P_b in the reaction vessel were recorded. The inlet valve was closed and the introduction of methane into the blind vessel was continued.
(6) Steps 4 and 5 were repeated until the equilibrium pressure reached 6.0 MPa.

2.3.4. Procedure for the Determination of Wax Separation Point. The wax separation point was determined by DSC method.[31,32] A French Setalam uDSC-7 microcalorimeter was used.

Specifically, the testing was done as follows:

(1) About 50 μg of crude oil was introduced into the sample chamber of the microcalorimeter.
(2) The temperature of crude oil was raised to 50 °C at a heating rate of 2 °C/min.
(3) After maintaining for 2 h, the temperature of crude oil was decreased to −20 °C at a cooling rate of 0.5 °C/min. The wax precipitated during the cooling process.
(4) As the temperature decreased, the point on the heat flow curve where it began to deviate from the baseline was the wax precipitation temperature.

2.3.5. Data Processing Methods. This section mainly describes the calculation methods for water conversion rate during hydrate formation in wax-containing oil−water systems.

At a temperature of 10.05 °C and pressure of 6.05 MPa, the solubility of methane in water was 1.585×10^{-3} (molar ratio). Compared with the solubility of methane in oil, which could be neglected, only the solubility of methane in oil was considered in the experiment.

The volume of air intake in the sapphire autoclave can be calculated by eq 1:

$$N_{in} = \frac{P_{b,0}V_b}{Z_{b,0}RT} - \frac{P_{b,1}V_b}{Z_{b,1}RT} \quad (1)$$

In the above equation, the subscript b represents the blind vessel. $P_{b,0}$ and $P_{b,1}$ correspond to the compressibility factors $Z_{b,0}$ and $Z_{b,1}$, respectively. The compressibility factors are calculated using the BWRS state equation. V_b is the volume of the blind vessel, R is the molar gas constant, and T is the experimental temperature.

At time t, the remaining gas in the sapphire autoclave is calculated by eq 2:

$$N_{g,t} = \frac{P_{g,t}V_{g,t}}{Z_{g,t}RT} \quad (2)$$

where, $P_{g,t}$ is the pressure of gas in the sapphire autoclave at time t, $Z_{g,t}$ is the compressibility factor of gas at time t, and $V_{g,t}$ is the gas volume. In the experiment for methane solubility in white oil, $P_{k,1}$ represents the pressure after adsorption equilibrium, and N_{in}-$N_{g,t}$ represents the molar quantity of methane dissolved in white oil. In the experiment for hydrate formation in wax-containing system, due to volume expansion during hydrate formation, the volume expansion coefficient of methane hydrate is 1.25. Hence, the gas volume in the sapphire autoclave at time t is calculated by Equation 3:

$$V_{g,t} = V_k - V_s - V_w(1 - x_t) - 1.25V_w x_t \quad (3)$$

where, V_k is the volume inside the sapphire autoclave, V_s is the volume of the circular iron piece used for stirring, V_w is the initial volume of water, and x_t is the water conversion rate.

Assuming the hydrate number of methane hydrate is 6,[6] the gas storage of hydrate at time t is calculated by eq 4:

$$N_{h,t} = \frac{m_w x_t}{18 \cdot 6} \quad (4)$$

where the initial mass of water is m_w, and the molar mass is considered as 18. The gas inside the sapphire autoclave complies with the mass conservation equation, as shown below.

$$N_{in} = N_{g,t} + N_{h,t} + N_a \quad (5)$$

where N_a represents the quantity of methane gas dissolved in white oil. Linear regression model with the least-squares method was used to obtain the isothermal adsorption line from 0 to 6.0 MPa at 275.15 K, represented by eq 6, where V_0 is the volume of the white oil.

$$N_a = 1000(0.2325 \times 10^{-6}P_{g,t} - 0.0551)V_0 \quad (6)$$

The solution of simultaneous eqs 2 to 5 can be used to derive the conversion rate of water.

$$x_t = \left[N_{in} - N_a - \frac{P_{g,t}(V_k - V_s - V_m)}{Z_{g,t}RT}\right] \Big/ \left(\frac{m_w}{108} - \frac{0.25P_{g,t}V_w}{Z_{g,t}RT}\right) \quad (7)$$

The solution of simultaneous eqs 1 to 7 can be used to calculate the conversion rate of water in the oil−water system at time t.

3. RESULTS AND DISCUSSION

3.1. The Effect of Wax on the Rate of Hydrate Formation in Oil−Water Systems. *3.1.1. Solubility of Methane in White Oil.* Following the experimental procedures described in Section 2.3.2, the solubility of methane in white oil was determined. The solubility curve was fitted to calculate the water conversion rate. Figure 3 shows the isothermal solubility curve of methane in white oil at 2 °C (up to 6.2 MPa). As shown in the figure, as the pressure increased, the solubility of methane in white oil increased linearly. Through least-squares fitting, the solubility curve equation can be obtained as follows:

https://doi.org/10.1021/acsomega.4c04920
ACS Omega 2024, 9, 31173−31184

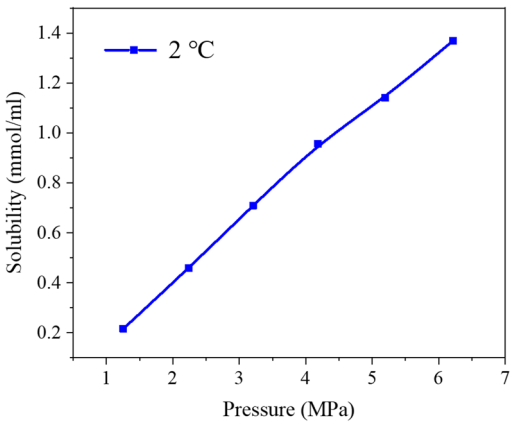

Figure 3. Isothermal solubility curve of methane in white oil.

$$S = \alpha P + \beta \quad (8)$$

where, S is the solubility in mmol/mL and P is the solution equilibrium pressure, in MPa. The solubility curve parameters α and β are presented in Table 2.

Table 2. Solubility Curve Parameters of Methane in White Oil

Temperature/°C	α	β
2	0.2325	−0.0551

3.1.2. Effect of Moisture Content on the Rate of Hydrate Formation in Different Wax-Containing Systems. This Experimental sSection examines the kinetics of formation of methane hydrate in white oil and water systems with different moisture contents and different wax contents at 2 °C and an initial pressure of 6.0 MPa. Experimental conditions and results are listed in Table 3.

Figure 4 shows the curve for rate of methane hydrate formation in white oil + water, with different moisture contents without wax, which corresponded to runs 1−5 in Table 3. It was evident from the figure that as the water content decreased, the rate of hydrate formation gradually increased. Especially, when the water content was 5 vol %, the water conversion rate reached 73.72%, 100 min after the hydrate formation began. Moreover, the hydrate formation rate was much higher than those of other water contents. When the moisture content was in the range of 10−25 vol %, the hydrate formation rates were relatively close in the early stage and the difference in the formation rates did not increase gradually until 85 min after conversion. This was due to the fact that stirring could enhance the dispersion effect of water in the oil phase, although the oil−water system in this set of experiments did not contain surfactants. However, water could very easily stratify. As a result, when the moisture content was high, stirring could only hydrate the oil.

Table 3. Experimental Results for the Formation of Methane Hydrate under Different Experimental Conditions (T = 275.15 K, P = 6.0 MPa)

Run	Moisture contents (vol %)	Wax contents (wt %)	Induction time (min)	Dissolved gas content (mmol)	Water conversion rate 100 min (%)
1	5	0	9	22.16	73.72
2	10	0	7	21	42.58
3	15	0	6	19.33	37.83
4	20	0	6	18.47	36
5	25	0	6	17.14	31.52
6	5	1	10	22.33	65.81
7	5	3	13	22.4	64.85
8	5	5	21	21.61	59.45
9	20	1	7	18.56	33.72
10	20	3	13	18.67	27.32
11	20	5	17	18.5	26.69
12	10	1	17	20.66	41.53
13	15	1	17	19.42	35.19
14	25	1	7	17.42	29.19
15	10	5	18	21.29	31.68

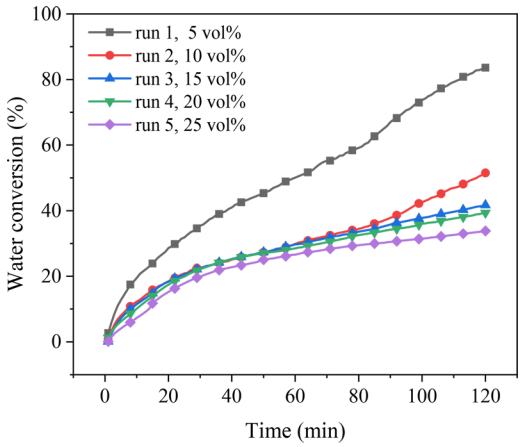

Figure 4. Conversion rate of water in the process of methane hydrate formation in white oil and water systems with different water contents.

The interface between the layers was disturbed and the major portion of water below the interface could not be effectively dispersed. For different moisture contents, the area of the oil−water interface in the columnar reactor was the same and hydrates were also mainly formed at the interface. Therefore, when the moisture content was >10 vol %, the rates of early hydrate formation were relatively closer. The proportion of water that could not be effectively dispersed below the oil−water interface was closely dependent on the moisture content. In other words, the greater the water content, the higher was the proportion of water that could not be effectively dispersed below the interface. This part of water was more difficult to form hydrates, which resulted in water content more than 10 vol %. The results showed that despite the increasing water content and hydrate formation, the water conversion rate is decreasing due to the limitation of gas mass transfer.

3.1.3. Kinetics of Hydrate Formation in Waxy Systems. 3.1.3.1. Effect of Wax Content on Rate of Hydrate Formation for Low Moisture Content. The kinetics study of methane hydrate formation in a white oil + water system with moisture content of 5 vol % and different wax contents was conducted. The experimental temperature was 2 °C and the initial pressure was 6.0 MPa, which corresponded to runs 6−8 in Table 3. Here, the viscosities of white oil−water systems with different wax contents were measured at 20 °C, shown in Table 4. As the wax content increasing, the viscosity of the systems increased, which may influence the hydrate formation. The curve for the formation rate of methane hydrate is shown

https://doi.org/10.1021/acsomega.4c04920
ACS Omega 2024, 9, 31173−31184

Table 4. Viscosities of White Oil + Water Systems with Different Wax Contents

Wax content (wt %)	Viscosity (mPa s)
0	40.9
1.0	174
3.0	657
5.0	1330

in Figure 5. From Figure 5 and Table 3, it was evident that as the wax content increased, the rate of hydrate formation

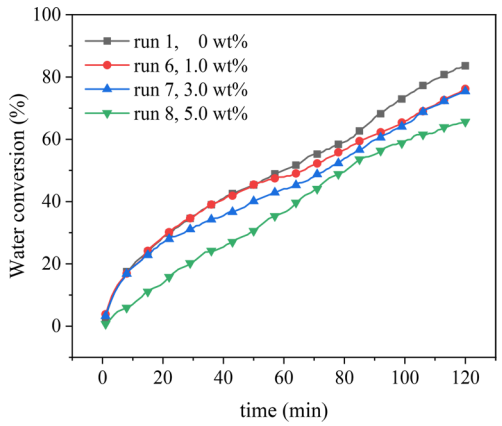

Figure 5. Formation rate of methane hydrate in the white oil and water system with different wax contents when the moisture content was 5 vol %.

gradually decreased. For <5.0 wt % wax content, the conversion rates of water at 100 min in run 6 and run 7 were 65.81% and 64.85%, respectively, which were relatively closer. For 5.0 wt % wax content, the conversion rate of water at 100 min dropped to 59.45%. This could be attributed to the wax would be dispersed in water, which would reduce the surface of water, thus improving the hydrate formation rate and water conversion rate. When the concentration of was in the system, the hydrate formation rate would be also accelerated, and the water conversion would be reduced, which might be due to excessive wax crystals in the system, causing inhibition of gas molecular mass transfer.[15]

Figure 6 shows the photographs depicting the changes before and after hydrate formation in oil−water systems with different wax contents for low water content. In the figure, the oil−water stratification in the reactor was obvious before hydrate formation and the viscosity of oil phase increased significantly with increase in wax content. When the wax content was ≤3.0 wt %, aggregation of hydrates occurred after they were formed, which were mainly deposited at the bottom and wall of the reactor. However, when the wax content was 5.0 wt %, the generated hydrates did not form obvious aggregates. This shows that high concentration of wax particles in the system acts as a physical barrier against the formation of hydrate particles, which prevents the aggregation of hydrates. It could be related to the wax precipitation, which was consistent with the previous study: when hydrate formation preceded the wax precipitation, the wax significantly reduces the aggregation of hydrate particles, thus improving the flow characteristics of the hydrate slurry.[33] However, as the wax content increased to 5.0 wt %, the stirrer could not even stir the generated hydrate slurry, since the viscosity of the system increased. Therefore, although a high wax content helped to disperse the hydrate particles, the viscosity of the system increased and the stirring efficiency decreased, resulting in a decrease in the hydrate formation rate when the wax content was high.

3.1.3.2. Effect of Wax Content on the Rate of Hydrate Formation with High Water Content. The kinetics study of hydrate formation of white oil + water system with moisture content of 20 vol % and different wax contents was conducted. The wax contents were 1.0, 3.0, and 5.0 wt %. The corresponding curves for formation rate of hydrates are shown in Figure 7, which corresponded to runs 9−11 in Table 3.

From Figure 7 and Table 3, it was evident that the conversion rate of water for high moisture content decreased with an increase in wax content, which was consistent with the

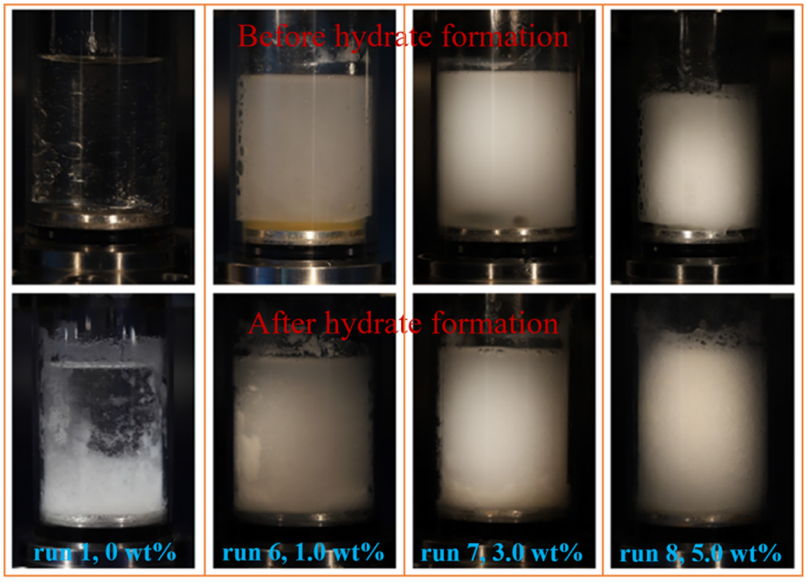

Figure 6. Photographs before and after the formation of methane hydrate in the white oil + water systems with different wax contents and low moisture content.

https://doi.org/10.1021/acsomega.4c04920
ACS Omega 2024, 9, 31173−31184

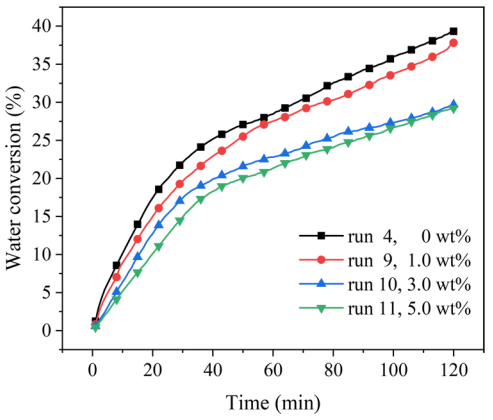

Figure 7. Conversion rate of water in the formation process of methane hydrate in white oil + water system with different wax contents, when the moisture content was 20 vol %.

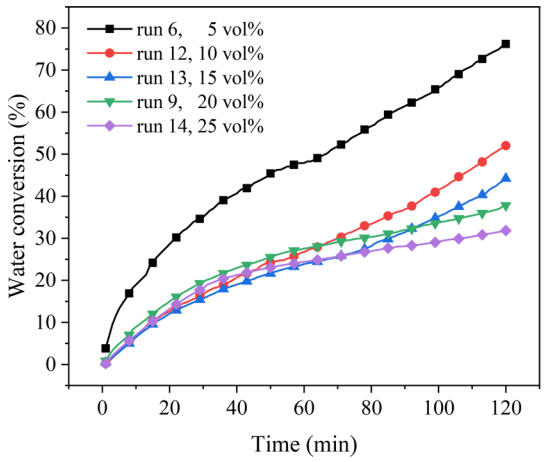

Figure 9. Conversion rate of water during the formation of methane hydrate in white oil + water systems with different moisture contents and 1.0 wt % wax.

law of formation rate of hydrates with low moisture content. Figure 8 shows the photographs depicting the changes before and after hydrate formation in oil + water systems with different wax contents having high water content. It was evident that when the moisture content was higher, the accumulation of hydrates at the bottom and walls of the kettle was more obvious. Similar to the system with low moisture content, as the wax content increasing, the fluidity of the white oil decreased, resulting in the stirring efficiency decreasing and the hydrate formation rate reducing.

3.1.3.3. Effect of Moisture Content on the Rate of Hydrate Formation with Low Wax Content. The experiment determined the formation rate of hydrates in white oil + water systems with different moisture contents when the wax content was 1.0 wt %. The curve for formation rate of hydrate is shown in Figure 9, which also corresponded to runs 6, 9, and 12−14 in Table 3. From Figure 9 and Table 3, it was evident that when the wax content was low, the formation rate of hydrate decreased as the water content increased. This was consistent with the trend of the formation rate of hydrate in the absence of wax. Figure 10 compares the hydrate formation rates when the wax content was 1.0 wt % and wax was absent (moisture contents were 5 vol %, 10 vol %, and 20 vol %). It was evident from the figure that in an oil−water mixture with 5 vol % moisture, 50 min after the hydrates began to form, the hydrate formation rate in the system containing 1.0 wt % wax was significantly higher than that in the system without wax. For 10 vol % and 20 vol % moisture contents, the hydrate formation rate without wax was closer to that when the wax content was 1.0 wt %, indicating that low wax content had little effect on the hydrate formation rate.

3.1.3.4. Effect of Moisture Content on Hydrate Formation Rate Having High Wax Content. The kinetics study of hydrate formation in the white oil + water system with 5.0 wt % wax content and different water contents was conducted. The corresponding curve for hydrate formation rate is shown in Figure 11, which corresponded to runs 8, 11, and 15. It was evident from the figure that when the wax content was high, the hydrate formation rate also decreased as the moisture

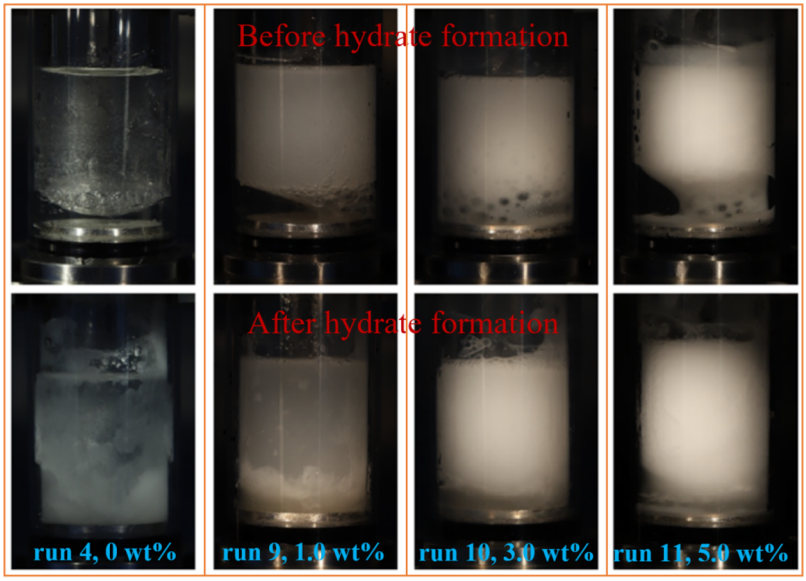

Figure 8. Photographs taken before and after the formation of methane hydrate in the white oil + water system having different wax contents and high water content.

https://doi.org/10.1021/acsomega.4c04920
ACS Omega 2024, 9, 31173−31184

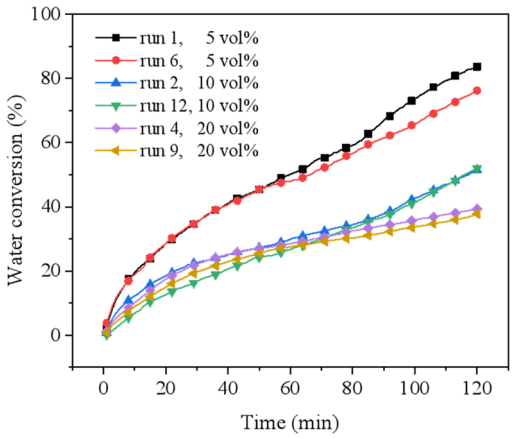

Figure 10. Comparison of water conversion rates in the formation process of methane hydrate in white oil + water systems with different moisture contents without wax and 1.0 wt % wax.

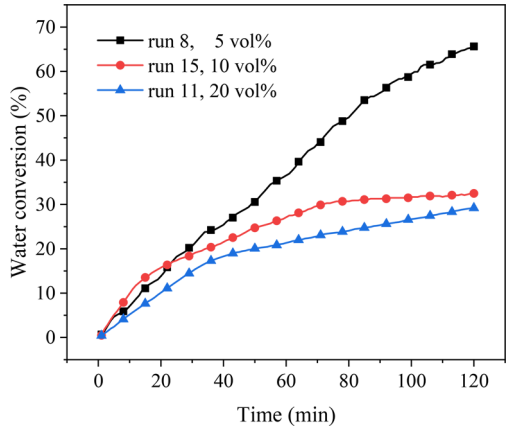

Figure 11. Conversion rate of water during the formation of methane hydrate in white oil + water systems with 5.0 wt % wax content and different moisture contents.

content increased. Figure 12 compares the hydrate formation rates in a system with 5.0 wt % wax content and a system without wax. It was clear that with a high wax content, the hydrate formation rate was significantly lower than that of a system without wax. At the same time, as compared with

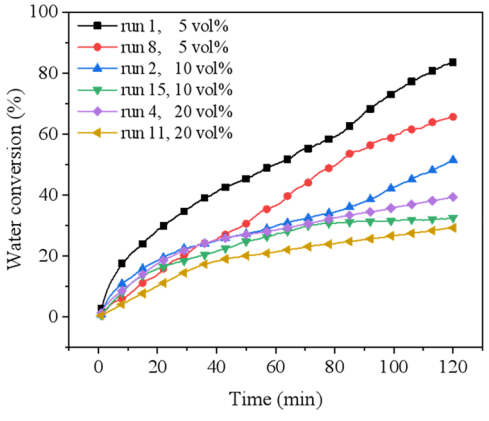

Figure 12. Comparison of water conversion rates in the formation process of methane hydrate in white oil + water systems with different moisture contents without wax and with 5.0 wt % wax.

Figure 10, reduction in the formation rate of hydrate due to high wax content was greater than that caused by low wax content. It could be related to the viscosity of the system being higher as the wax content increases, resulting in the stirring efficiency decreasing, and the mass transfer of gas during the hydrate formation process being inhibited, leading to a lower hydrate formation rate.

3.1.3.5. Effect of Wax on the Induction Period during Hydrate Formation. Figure 13 shows the induction periods of hydrate formation for different wax contents in oil + water systems with low moisture content and high moisture content. As shown in the figure, for 5 vol % and 20 vol % moisture, the induction time during hydrate formation increased as the wax content increased. Literature references[24,34] also indicated that the induction time for hydrate formation increased with increase in wax content. This could be attributed to the uniform distribution of wax crystals in the oil phase that hindered the diffusion of gas phase to the water droplet surface and thus prolonged the induction time for hydrate formation.[24,35] In this study, as the wax content increased, the viscosity of the oil + water mixture increased significantly, the stirring efficiency decreased, and the dissolution process of gas in the oil phase slowed down, which resulted in a prolonged induction time for hydrate formation.

3.2. Influence of Hydrate Formation on the Thermodynamic Behavior of Wax Crystal Precipitation.

3.2.1. Determination of Wax Precipitation Point of White Oil in Hydrate. A microcalorimeter was employed to study the influence of hydrate formation on the thermodynamic behavior of precipitation of wax crystal. The freezing point of the selected white oil was measured in order to determine whether the precipitation of crystals that occurred in the white oil was within the temperature range of the experiment. Figure 14 shows the temperature-heat flow plots of white oil when cooled from 60 °C to −15 °C. During temperature reduction, no obvious exothermic peak appeared, indicating that the white oil did not solidify during the process. Therefore, the white oil was applicable in the temperature range of 2−8 °C tested as a part of this study.

3.2.2. Determination of Average Precipitation Heat of Wax. The heat of wax crystal precipitation during the cooling process was measured, and Figure 15 shows the corresponding temperature-heat flow plots. In the heat flow plots, an exothermic peak and an endothermic peak appeared when the temperature was reduced from 60 °C to −15 °C and during the heating process, respectively. They corresponded to the precipitation and dissolution processes of wax crystals in the white oil, respectively. Due to the groups of wax crystals, the carbon number distribution was not uniform, and peak shape showed tailing. Integration of the heat flow peak of wax crystals when they redissolved during the heating process and then dividing it by the total wax content provided the average heat of precipitation of wax crystals, which was 143.11 J/g. This value was used for subsequent calculation of the rate of precipitation of wax crystals.

3.2.3. Determination of Precipitation Rate of Wax Crystals after Hydrate Formation. In Figure 15, at the beginning or end of cooling, a heat flow peak was generated. For the conventional research temperature range of 2−8 °C, these two heat flow peaks would interfere, so the temperature range of the study needed to be expanded. For methane hydrate, its formation pressure at 8 °C was 5.85 MPa. When the temperature rose to 15 °C, the phase equilibrium pressure

https://doi.org/10.1021/acsomega.4c04920
ACS Omega 2024, 9, 31173−31184

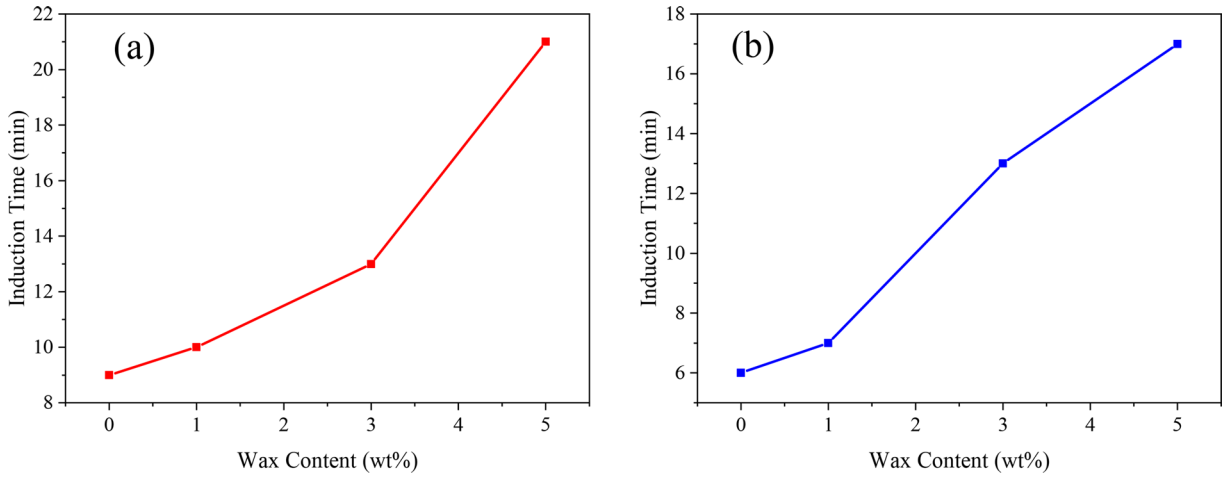

Figure 13. Variations in the induction period for the formation of methane hydrate in the white oil + water system with the wax content: (a) moisture content was 5 vol %, (b) moisture content was 20 vol %.

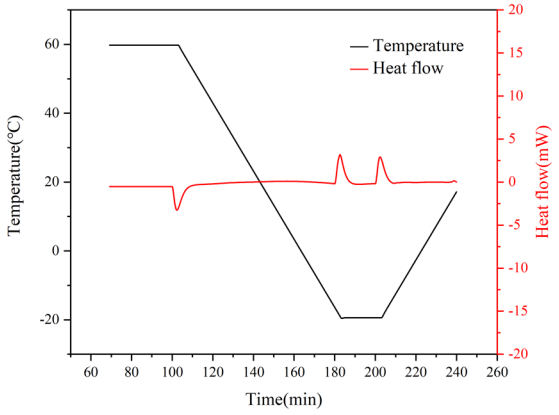

Figure 14. Temperature-heat flow plots during the cooling process of white oil.

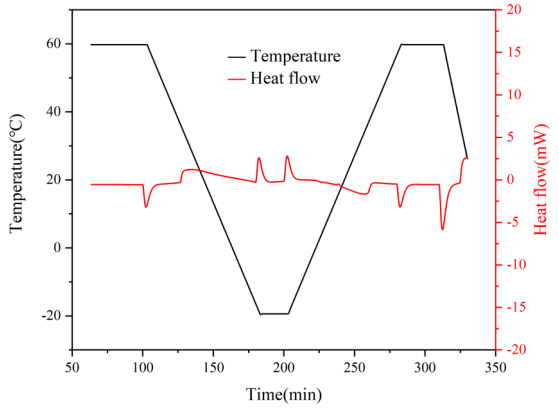

Figure 15. Temperature-heat flow plots during the cooling process of white oil containing 20 wt % wax.

increased correspondingly to 12.86 MPa, and the experimental pressure was too high. Therefore, in this study, thermodynamic accelerator was added to reduce the pressure of hydrate formation. Tetrahydrofuran was chosen as the thermodynamic accelerator, its content in water was 5.56 mol %, and the initial gas pressure was 6.0 MPa.

First, the aqueous tetrahydrofuran solution and white oil were mixed to obtain an oil−water mixture and transferred to the DSC reactor. Then, the temperature was set to 20 °C. By continuously fluctuating the temperature between −15 and 5 °C, all the water was converted into hydrates. Then, the temperature was raised to 25 °C and then cooled to 0 °C at a rate of 1 °C/min. The exothermic peak in the range of 20−5 °C was used to calculate the wax precipitation rate. The mass percentage of wax crystal precipitation was calculated using the following formula,

$$\varphi = \frac{\int_{20}^{T} \mathrm{d}Q/\overline{Q}}{m_0} 100\% \tag{9}$$

where, T is the difference in temperature points, which indicated the average precipitation heat of wax (143.11 J/g) and m_0 is the initial weight of wax in white oil. The above formula represented the mass percentage of precipitated wax to the total mass in the temperature range from 20 °C to the target temperature T.

Figure 16 shows the wax precipitation curves after hydrate formation in the white oil + water systems with different wax contents and having moisture content of 5 vol %. The

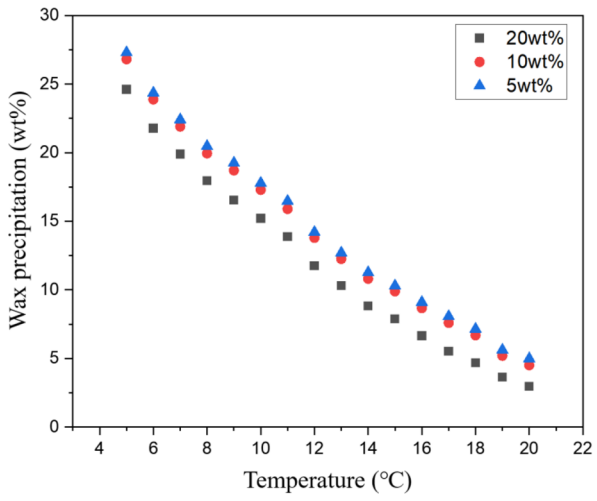

Figure 16. Wax precipitation curves after hydrate formation in white oil + water systems with different wax contents and water content of 5 vol %.

https://doi.org/10.1021/acsomega.4c04920
ACS Omega 2024, 9, 31173−31184

precipitation curve of wax appeared relatively smooth, which was slightly different from the S-shaped curve in some studies, as the wax distribution range of carbon number used in this study was narrow and also the temperature range in this study was narrow. As the initial wax content increased, within the temperature range measured experimentally, the percentage of wax precipitation was relatively low. This could be due to the fact that when the wax content was greater, there were more nucleation points for wax in the early stage, and so more wax was produced in the early stage of cooling (greater than 20 °C).[36] Hence, the precipitation was less within the measured temperature range. When the wax content was reduced to 10 and 5 wt %, the percentage of wax crystals precipitated was relatively closer. Compared with the precipitation percentage of wax crystals reported in literature, the value in this study was lower, mainly as the experiments in this study were conducted in the temperature range of 20 to 5 °C, while some literature measured the amount from the wax precipitation point. Since this experiment wanted to ensure that the hydrates were formed first, the measurement could not be started from the wax precipitation point.

The wax precipitation rate after hydrate formation in white oil + water systems with different wax contents and 10 vol % water content was determined. Figure 17 shows the

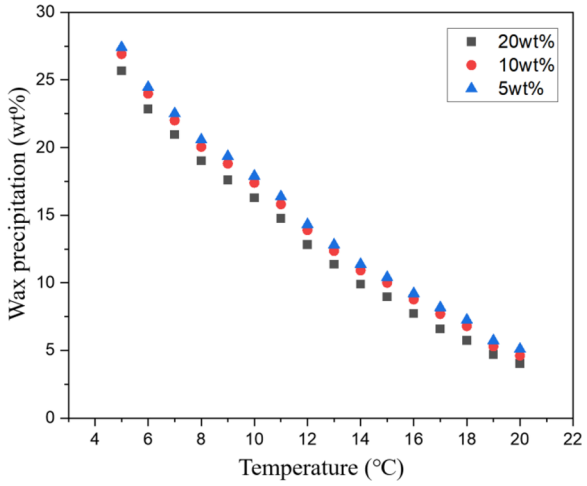

Figure 17. Wax precipitation curves after hydrate formation in white oil + water systems with different wax contents and 10 vol % water.

corresponding wax precipitation curves. From the figure, it was clear that as the initial wax content increased, the percentage of wax precipitation gradually decreased in the temperature range of 20−5 °C. However, the wax precipitation curves for initial wax contents of 20 and 10 wt % with 10 vol % moisture were closer, as compared with the corresponding curves for 5 vol % moisture. This could be due to the fact that when the water content increased, the volume of the oil phase in the oil−water system decreased (the loading volume in the DSC kettle was required to be kept constant), and the hydrates in the system occupied more volume. Therefore, when the temperature was higher than 20 °C, the amount of wax precipitated in the oil−water system with an initial wax content of 20 wt % was relatively reduced. This ultimately led to the precipitation of wax in several systems with different initial wax contents in the temperature range of 20−5 °C. The percentages were closer.

For white oil with different wax contents and moisture content of 15 vol %, the wax precipitation curves after hydrate formation are shown in Figure 18. Similar to the case of 5 and

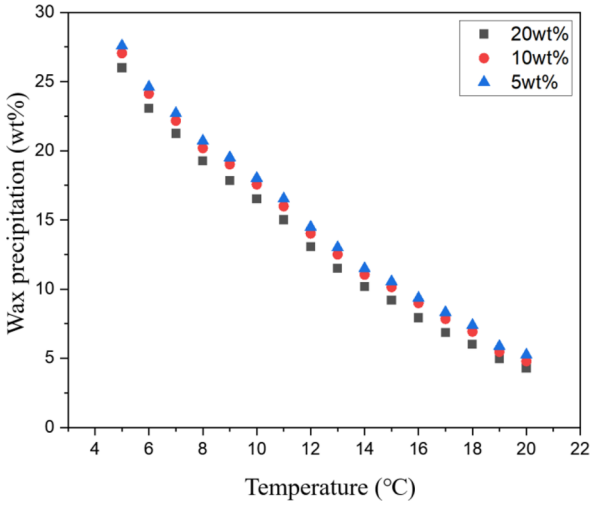

Figure 18. Wax precipitation curves after hydrate formation in white oil−water systems with different wax contents and 15 vol % water.

10 vol % water, when the initial wax content was higher, the percentage of wax precipitation was relatively low. However, when the water content was relatively low, the amounts of wax precipitated under different initial wax contents were closer.

4. CONCLUSIONS

Wax and hydrates coexist under low-temperature and high-pressure conditions, mutually influencing each other thermodynamically and kinetically. Wax would affect hydrate formation rates, while hydrates influence wax crystal precipitation rates.

(1) With 5 vol % water, the water conversion rate reached 73.72% within 100 min of hydrate formation onset, showing a significantly higher formation rate than other water contents. For 10 to 25 vol % water, initial hydrate formation rates were similar, with differences emerging only after 85 min.

(2) Before hydrate formation, the oil−water mixture showed stratification. Increased wax content significantly raised the mixture's viscosity, slowing gas dissolution in the oil phase and extending the induction time for hydrate formation.

(3) Wax in the oil phase reduced hydrate formation rates, especially at higher wax contents. In high wax content systems, more wax precipitated initially, with over 70% precipitating before hydrate formation, leading to less precipitation within the hydrate formation temperature range.

(4) Low water content increased nucleation points for wax crystals in the oil phase, resulting in greater differences in precipitation rates among various wax contents. For water contents above 10%, the differences in precipitation rates between different wax contents were less significant, indicating a reduced impact of water content on wax precipitation rates.

The hydrophilic nature of hydrates minimally influenced wax crystal nucleation and growth. Generally, wax crystals

https://doi.org/10.1021/acsomega.4c04920
ACS Omega 2024, 9, 31173−31184

precipitate before hydrates, necessitating control measures for wax deposition during production processes. Future work should be carried out to explore the interaction mechanism of wax and hydrate under different conditions, optimize the control strategy for wax deposition and hydrate formation, establish a computational model to simulate the formation process of wax and hydrate under different conditions, and predict and optimize the production parameters.

AUTHOR INFORMATION

Corresponding Authors

Huiyong Liang − *Ningbo Institute of Dalian University of Technology, Ningbo 315016, China;* orcid.org/0000-0001-9448-1033; Email: lianghuiyong@dlut.edu.cn

Xin Lv − *Ningbo Institute of Dalian University of Technology, Ningbo 315016, China*; Email: lvxin@dlut.edu.cn

Authors

Jinghua Chen − *State Key Laboratory of Offshore Natural Gas Hydrates, Beijing 100028, China; China National Offshore Oil Corporation Research Institute Co. LTD, Beijing 100028, China*

Haihong Chen − *State Key Laboratory of Offshore Natural Gas Hydrates, Beijing 100028, China; China National Offshore Oil Corporation Research Institute Co. LTD, Beijing 100028, China*

Shi Shen − *Ningbo Institute of Dalian University of Technology, Ningbo 315016, China*

Haiyuan Yao − *State Key Laboratory of Offshore Natural Gas Hydrates, Beijing 100028, China; China National Offshore Oil Corporation Research Institute Co. LTD, Beijing 100028, China*

Rui Qin − *State Key Laboratory of Offshore Natural Gas Hydrates, Beijing 100028, China; China National Offshore Oil Corporation Research Institute Co. LTD, Beijing 100028, China*

Yang Ge − *State Key Laboratory of Offshore Natural Gas Hydrates, Beijing 100028, China; China National Offshore Oil Corporation Research Institute Co. LTD, Beijing 100028, China*

Ting Huang − *State Key Laboratory of Offshore Natural Gas Hydrates, Beijing 100028, China; China National Offshore Oil Corporation Research Institute Co. LTD, Beijing 100028, China*

Complete contact information is available at: https://pubs.acs.org/10.1021/acsomega.4c04920

Notes

The authors declare no competing financial interest.

ACKNOWLEDGMENTS

This study was supported by the State Key Laboratory of Offshore Natural Gas Hydrates (2022-KFJJ-SHW), the Zhejiang Provincial Natural Science Foundation (Grant No. LQ24E060008), the National Natural Science Foundation of China (Grant No. 52306188).

REFERENCES

(1) Elkatory, M. R.; Soliman, E. A.; El Nemr, A.; Hassaan, M. A.; Ragab, S.; El-Nemr, M. A.; Pantaleo, A. Mitigation and remediation technologies of waxy crude oils' deposition within transportation pipelines: a review. *Polymers* **2022**, *14* (16), 3231.

(2) Kiyingi, W.; Guo, J.-X.; Xiong, R.-Y.; Su, L.; Yang, X.-H.; Zhang, S.-L. Crude oil wax: A review on formation, experimentation, prediction, and remediation techniques. *Petroleum Science* **2022**, *19* (5), 2343−2357.

(3) Radulescu, A.; Schwahn, D.; Stellbrink, J.; Kentzinger, E.; Heiderich, M.; Richter, D.; Fetters, L. J. Wax crystallization from solution in hierarchical morphology templated by random poly (ethylene-co-butene) self-assemblies. *Macromolecules* **2006**, *39* (18), 6142−6151.

(4) Santos, G.; Daraboina, N.; Sarica, C. Dynamic Microscopic Study of Wax Deposition: Particulate Deposition. *Energ Fuel* **2021**, *35* (15), 12065−12074.

(5) Gao, S. Investigation of Interactions between Gas Hydrates and Several Other Flow Assurance Elements. *Energ Fuel* **2008**, *22* (5), 3150−3153.

(6) Sloan, E. D.; Koh, C. A. *Clathrate Hydrates of Natural Gases*; CRC Press, 2007.

(7) Feng, Y.; Han, Y.; Gao, P.; Kuang, Y.; Yang, L.; Zhao, J.; Song, Y. Study of hydrate nucleation and growth aided by micro-nanobubbles: Probing the hydrate memory effect. *Energy* **2024**, *290*, No. 130228.

(8) Hammerschmidt, E. G. Formation of Gas Hydrates in Natural Gas Transmission Lines. *Industrial & Engineering Chemistry* **1934**, *26* (8), 851−855.

(9) Sloan, E. D. *Natural Gas Hydrates in Flow Assurance*; Gulf Professional Publishing, 2010.

(10) Sayani, J. K. S.; Pedapati, S. R.; Kassim, Z.; Lal, B. Investigation on Thermodynamic Equilibrium Conditions of Methane Hydrates in Multiphase Gas-Dominant Pipelines. *Acs Omega* **2021**, *6* (4), 2505−2512.

(11) Liang, H.; Guan, D.; Shi, K.; Yang, L.; Zhang, L.; Zhao, J.; Song, Y. Characterizing Mass-Transfer mechanism during gas hydrate formation from water droplets. *Chemical Engineering Journal* **2022**, *428*, No. 132626.

(12) Wang, J.; Meng, Y.; Han, B.; Liu, Z.; Zhang, L.; Yao, H.; Wu, Z.; Chu, J.; Yang, L.; Zhao, J.; et al. Hydrate blockage in subsea oil/gas flowlines: Prediction, prevention, and remediation. *Chemical Engineering Journal* **2023**, *461*, No. 142020.

(13) Kinnari, K.; Hundseid, J.; Li, X.; Askvik, K. M. Hydrate Management in Practice. *Journal of Chemical & Engineering Data* **2015**, *60* (2), 437−446.

(14) Sloan, E. D. Hydrocarbon hydrate flow assurance history as a guide to a conceptual model. *Molecules* **2021**, *26* (15), 4476.

(15) Guo, P.; Song, G.; Ning, Y.; Li, Y.; Wang, W. Investigation on Hydrate Growth at Oil−Water Interface: In the Presence of Wax. *Energ Fuel* **2021**, *35* (15), 11884−11895.

(16) Zhang, J.; Li, C.; Yang, F.; Shi, L.; Yao, B.; Sun, G. Study on the influence mechanism of the interaction between waxes and asphaltenes on hydrate growth. *Fuel* **2023**, *338*, No. 127322.

(17) Theyab, M. A. Fluid flow assurance issues: literature review. *SciFed J. Petroleum* **2018**, *2* (1), 1−11.

(18) Wang, W.; Huang, Q.; Zheng, H.; Wang, Q.; Zhang, D.; Cheng, X.; Li, R. Effect of wax on hydrate formation in water-in-oil emulsions. *J. Dispersion Sci. Technol.* **2020**, *41* (12), 1821−1830.

(19) Ellison, B.; Gallagher, C.; Frostman, L.; Lorimer, S. the Physical Chemistry of Wax, Hydrates, And Asphaltene. In *Offshore Technology Conference 2000* ; OTC, 2000; OTC-11963-MS.

(20) Zhang, D.; Huang, Q.; Zheng, H.; Wang, W.; Cheng, X.; Li, R.; Li, W. Effect of wax crystals on nucleation during gas hydrate formation. *Energ Fuel* **2019**, *33* (6), 5081−5090.

(21) Wang, F.; Ma, R.; Xiao, S.; English, N. J.; He, J.; Zhang, Z. Anti-gas hydrate surfaces: perspectives, progress and prospects. *J. Mater. Chem. A* **2022**, *10* (2), 379−406.

(22) Song, G.; Ning, Y.; Li, Y.; Wang, W. Investigation on hydrate growth at the oil−water interface: In the presence of wax and kinetic hydrate inhibitor. *Langmuir* **2020**, *36* (48), 14881−14891.

(23) Yang, F.; Zhao, Y.; Sjöblom, J.; Li, C.; Paso, K. G. Polymeric Wax Inhibitors and Pour Point Depressants for Waxy Crude Oils: A Critical Review. *J. Dispersion Sci. Technol.* **2015**, *36* (2), 213−225.

(24) Chen, Y.; Shi, B.; Liu, Y.; Song, S.; Gong, J. Experimental and Theoretical Investigation of the Interaction between Hydrate Formation and Wax Precipitation in Water-in-Oil Emulsions. *Energ Fuel* **2018**, *32* (9), 9081−9092.
(25) Chen, Y.; Shi, B.; Fu, S.; Li, Q.; Yao, H.; Liu, Y.; Lv, X.; Wang, J.; Liao, Q.; Duan, X.; et al. Kinetic and rheological investigation of cyclopentane hydrate formation in waxy water-in-oil emulsions. *Fuel* **2021**, *287*, No. 119568.
(26) Liu, Z.; Li, Y.; Wang, W.; Song, G.; Lu, Z.; Ning, Y. Wax and Wax−Hydrate Deposition Characteristics in Single-, Two-, and Three-Phase Pipelines: A Review. *Energ Fuel* **2020**, *34* (11), 13350−13368.
(27) Ke, W.; Chen, D. A short review on natural gas hydrate, kinetic hydrate inhibitors and inhibitor synergists. *Chinese J. Chem. Eng.* **2019**, *27* (9), 2049−2061.
(28) Seyfaee, A.; Lashkarbolooki, M.; Esmaeilzadeh, F.; Mowla, D. Investigation of the effect of insulation on wax deposition in an Iranian crude oil pipeline with OLGA simulator. *J. Dispersion Sci. Technol.* **2012**, *33* (8), 1218−1224.
(29) Hu, Y.-Q.; Xie, J.; Xue, S.-N.; Xu, M.; Fu, C.-H.; He, H.-L.; Liu, Z.-Q.; Ma, S.-M.; Sun, S.-Q.; Wang, C.-L. Research and application of thermal insulation effect of natural gas hydrate freezing corer based on the wireline-coring principle. *Petroleum Science* **2022**, *19* (3), 1291−1304.
(30) Duffy, D.; Moon, C.; Rodger, P. Computer-assisted design of oil additives: hydrate and wax inhibitors. *Mol. Phys.* **2004**, *102* (2), 203−210.
(31) Espada, J. J.; Coutinho, J. A. P.; Peña, J. L. Evaluation of Methods for the Extraction and Characterization of Waxes from Crude Oils. *Energ Fuel* **2010**, *24* (3), 1837−1843.
(32) Zaky, M. T.; Mohamed, N. H. Comparative study on separation and characterization of high melting point macro- and micro-crystalline waxes. *J. Taiwan Inst Chem. E* **2010**, *41* (3), 360−366.
(33) Liu, J.; Wang, J.; Dong, T.; Liang, D. Effects of wax on CH4 hydrate formation and agglomeration in oil−water emulsions. *Fuel* **2022**, *322*, No. 124128.
(34) Zheng, H.; Huang, Q.; Wang, W.; Long, Z.; Kusalik, P. G. Induction Time of Hydrate Formation in Water-in-Oil Emulsions. *Ind. Eng. Chem. Res.* **2017**, *56* (29), 8330−8339.
(35) Liu, Y.; Shi, B.; Ding, L.; Ma, Q.; Chen, Y.; Song, S.; Zhang, Y.; Yong, Y.; Lv, X.; Wu, H.; et al. Study of hydrate formation in water-in-waxy oil emulsions considering heat transfer and mass transfer. *Fuel* **2019**, *244*, 282−295.
(36) Wang, H.; Boyer, S. A. E.; Bellet, M.; Dalle, F. Effects of Wax Components and the Cooling Rate on Crystal Morphology and Mechanical Properties of Wax−Oil Mixtures. *Cryst. Growth Des* **2023**, *23* (3), 1422−1433.

https://doi.org/10.1021/acsomega.4c04920
ACS Omega 2024, 9, 31173−31184